J Mater Sci (2008) 43:1979–1986
DOI 10.1007/s10853-007-2431-y

Comparison study on the size and phase control of nanocrystalline TiO_2 in three Ti–Si oxide structures

Lu-Yan Wang · Yan-Ping Sun · Bing-She Xu

Received: 17 July 2007 / Accepted: 26 December 2007 / Published online: 1 February 2008

Abstract Three types of Ti–Si binary oxides have been prepared by sol-gel processes. The effects of SiO_2 addition and annealing temperature on the grain size, phase transition, dispersion, and microstructure of nanocrystalline (nc) TiO_2 anatase in the three Ti–Si oxide structures have been comparatively investigated by X-ray diffraction (XRD) analysis and high-resolution transmission electron microscopy (HRTEM). The grain growth and anatase-rutile transformation (ART) of $ncTiO_2$ were found to depend not only on the SiO_2 content and annealing temperature, but also on the composite structure. Both the grain growth and the ART of $ncTiO_2$ proved to be significantly inhibited with increasing SiO_2 content for all of the Ti–Si samples, but the structure of intimately mixed Ti–Si binary oxide showed the best inhibiting ability under high-temperature annealing. This result might be attributed to variations in the large lattice strains in $ncTiO_2$, which were mainly induced by the substitution of Ti^{4+} by Si^{4+}. Plausible mechanisms for the grain growth and ART of $ncTiO_2$ are proposed. To inhibit the grain growth of $ncTiO_2$, the addition of 10 and 30 mol% SiO_2 proved to be optimal for Ti–Si samples annealed at 773 K and 1273 K, respectively.

L.-Y. Wang · Y.-P. Sun (✉)
Chemical Engineering Department, Taiyuan University of Technology, No. 79# Yingze West Street, Taiyuan 030024, China
e-mail: ypsun@tyut.edu.cn

L.-Y. Wang
e-mail: xgz_good2006@126.com

B.-S. Xu
Key Laboratory of Interface and Engineering in Advanced Material, Ministry of Education, Taiyuan University of Technology, No. 79# Yingze West Street, Taiyuan 030024, China

Introduction

The silica–titania composite system has recently attracted the interest of many researchers owing to its enhanced photocatalytic activity and superior photoinduced hydrophilicity compared with those of pure TiO_2. According to these reports, the enhanced activities could be attributed to its high adsorptivity [1–4], a better dispersion effect of TiO_2 [5, 6], increased surface acidity [7, 8], changes in the TiO_2 structure [9, 10], and quantum-sized crystalline TiO_2 [11, 12]. It is known that the physical and chemical properties of TiO_2 in the nm size range are strongly influenced by phase composition, grain size, and degree of dispersion. These relationships are generally the same for silica–titania composites. However, the influencing factors and mechanisms that govern the phase transformation, grain growth, and degree of dispersion of $ncTiO_2$ are not completely understood for the silica–titania composite system. Moreover, there are currently many types of composite Ti–Si binary oxides [13–16], but few studies have compared these different types.

In the present work, three different Ti–Si binary oxides, namely silica-supported titania, intimately mixed silica–titania, and silica-coated titania, each in the form of nanocomposite powders containing 10–40 mol% SiO_2, have been prepared by sol-gel processes. As a reference, pure TiO_2 powder has also been prepared using the same procedure. X-ray diffraction (XRD) and high-resolution transmission electron microscopy (HRTEM) have been employed to compare variations in the $ncTiO_2$ in the three different Ti–Si oxide structures. These variations include crystal grain size, phase transition, degree of dispersion, and microstructure of the $ncTiO_2$. This comparison has identified the factors that control the crystal grain size and phase transition of $ncTiO_2$ in nanocomposite Ti–Si binary

oxides, and thus allows a better understanding of the mechanism involved.

Experimental

Tetrabutyl orthotitanate (TBOT) and tetraethyl orthosilicate (TEOS) were used as titania and silica precursors, respectively. Other chemicals included anhydrous ethanol (EtOH), doubly distilled water, hydrochloric acid (HCl, 37 wt.%), and acetylacetone (acac). All chemicals used were of analytical grade. Using TS110 as an example, samples were named as follows: TS represents composite titania–silica oxide, and the first numeral 1 indicates process 1 (2 and 3 denote processes 2 and 3, respectively); the last two numerals indicate an SiO_2 content of 10% added to the precursors, based on the molar ratio $x\% = [SiO_2/(TiO_2 + SiO_2)] \times 100\%$ (x = 10, 20, 30, 40). Chemical proportions used are shown in Table 1. The preparation processes for the three different Ti–Si binary oxides were as follows:

(1) Process 1, a two-step procedure for preparing silica-supported titania: TEOS was first pre-hydrolyzed with water, HCl, and EtOH at 313 K for approximately 2 h to form an SiO_2 sol; HCl, TBOT, EtOH, and water were then added dropwise at 273 K under vigorous stirring. After gelation, the product was dried at 353 K, ground to a fine powder, heated at 723, 873, 1173, or 1273 K for 3 h, and then cooled at room temperature.

(2) Process 2, a one-step procedure for preparing intimately mixed binary oxides [17]: First, acac was added to a solution of TBOT under vigorous stirring at ambient temperature to modify the reactivity of the titanium alkoxide through the formation of titanium alkoxide chelates. The resulting solution was then thoroughly mixed with TEOS, EtOH, HCl, and water at 313–323 K, in a similar manner to the last step of process 1.

(3) Process 3, a two-step procedure for preparing silica-coated titania: In brief, a TiO_2 sol was first prepared by mixing TBOT, acac, EtOH, HCl, and water at 313–323 K. HCl, TEOS, and water were then added, using a similar approach as in process 1.

Characterization

The prepared Ti–Si binary oxides were identified by powder XRD analysis on a Rigaku D/Max 2500 diffractometer with a Cu-K_α source (40 kV, 100 mA) at a scan rate of 8°/min with a step size of 0.01° for 2θ angles from 20° to 65°. The grain size (D) and unit-cell volume (V) of anatase, as well as the weight percentage of rutile (W_R), were calculated by applying the following three formulae (Eqs. (1–3)) [18, 19]:

$$D = \frac{0.89\lambda}{B_{1/2}\cos\theta} \tag{1}$$

$$V = a_0 \times b_0 \times c_0\ (a_0 = b_0),\ \frac{1}{d^2} = \frac{h^2}{a_0^2} + \frac{k^2}{b_0^2} + \frac{l^2}{c_0^2} \tag{2}$$

$$W_R = \frac{1}{(1 + 0.8I_A/I_R)} \times 100\% \tag{3}$$

where B is the peak width in radians at half the diffraction intensity of anatase (101); λ is the X-ray wavelength used; θ is the Bragg diffraction angle; a_0, b_0, and c_0 are the cell constants of ncTiO_2 anatase; h, k, and l are crystal plane indices given by the XRD data; d is the in-plane spacing; I_A and I_R are the integrated peak intensities of anatase (101) and rutile (110), respectively.

Variations in the size, dispersion, and microstructure of the TiO_2 crystal grains in the three types of Ti–Si binary

Table 1 Chemical proportions of the three types of Ti–Si binary oxides

Sample	SiO_2 (mol%)	TBOT (mmol)	TEOS (mmol)	HCl (mmol)	H_2O (mmol)	Acac. (mmol)
TS110	10	17.63	1.96	6.86	78.36	–
TS120	20	17.63	4.41	7.71	88.16	–
TS130	30	17.63	7.56	8.81	100.76	–
TS140	40	17.63	11.75	10.28	117.52	–
TS210	10	17.63	1.96	6.86	77.28	1.76
TS220	20	17.63	4.41	7.71	88.16	1.98
TS230	30	17.63	7.56	8.81	100.76	2.27
TS240	40	17.63	11.75	10.28	117.52	2.64
TS310	10	17.63	1.96	11.75	78.36	1.76
TS320	20	17.63	4.41	13.22	88.16	1.98
TS330	30	17.63	7.56	15.16	100.76	2.28

oxides were observed by HRTEM (JEM2010 electron microscope, Tokyo, Japan; 200 kV, Cs = 0.8 mm). A small amount of each sample was dispersed in ethanol and stirred in an ultrasonic bath for 30 min. Three or four drops of the dispersed samples were then placed on Cu grids for observation.

Results and discussion

Effect of SiO_2 addition on annealing at 773 K

X-ray diffraction patterns of Ti–Si binary oxides annealed at 773 K are shown in Fig. 1a–c; the mean crystal grain size calculated using the Scherrer formula (Eq. (1)) is shown in Fig. 1d. For each of the Ti–Si binary oxides with 10 mol% SiO_2, all peaks correspond to the anatase phase (2θ: 25.3°, 37.8°, 48.0°, 54.4°, and 62.8°) based on PDF#21-1272. No peaks corresponding to SiO_2 were observed. These data indicate that well ordered, long-range $ncTiO_2$ anatase is formed with a grain size of approximately 7–8 nm in each of the Ti–Si binary oxides; moreover, the SiO_2 is amorphous. This result agrees well with the HRTEM results. Representative HRTEM images of TS210 and TS310 annealed at 773 K are shown in Fig. 2. The images clearly reveal that well-ordered, long-range $ncTiO_2$ with a grain size of approximately 7–8 nm is formed and is generally well dispersed in an amorphous SiO_2 matrix, although these composite particles are somewhat aggregated. The Fourier-transform image shown in Fig. 2b clearly indicates (101), (112), (200), and (211) anatase reflections, and most crystal planes are oriented with the (101) plane. These results imply that the introduction of 10 mol% SiO_2 can effectively suppress the grain growth of $ncTiO_2$ anatase in the three Ti–Si oxide structures compared with pure $ncTiO_2$ (Fig. 1d). According to a previous investigation [20], the grain growth of $ncTiO_2$ is associated with the precursors of Ti and Si, and $ncTiO_2$ crystallizes with the cleavage of Ti–O–Si and organic combustion. Therefore, it is possible that the suppressed grain growth of $ncTiO_2$ anatase is related to the number of Ti–O–Si linkages.

For Ti–Si binary oxides with 30 and 40 mol% SiO_2, the XRD patterns show only one strong peak at the lower 2θ angle of 25.3°, which corresponds to the anatase phase. For Ti–Si binary oxides with more than 40 mol% SiO_2, no diffraction peak was detected. Similar results were obtained for all three Ti–Si oxide structures. As shown in Fig. 1d, the grain size of $ncTiO_2$, calculated by XRD, is seen to decrease with increasing SiO_2 content. The weakening and broadening of the XRD peaks appear to be caused by a decrease in the $ncTiO_2$ grain size. In fact, broad XRD peaks are commonly attributed to structural changes in samples, such as the formation of amorphous phases, large lattice strains in crystal grains, the formation of extremely fine particles, or the embedding of very small crystals in an amorphous matrix [21]. Therefore, for the Ti–Si binary oxides with 30–40 mol% SiO_2, the calculated

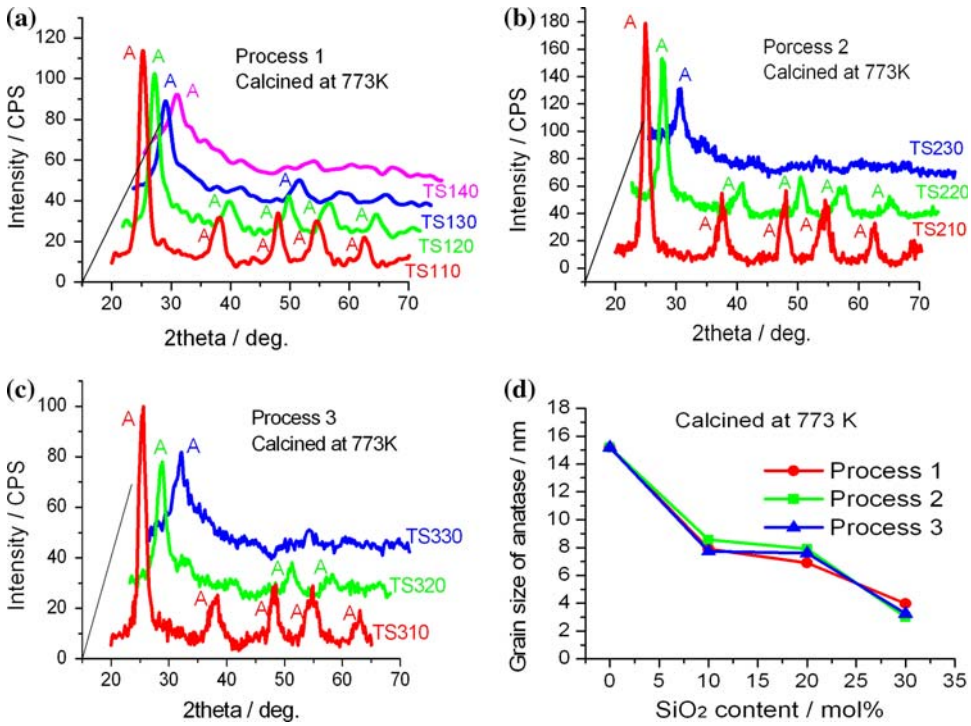

Fig. 1 XRD patterns for Ti–Si binary oxides annealed at 773 K: (**a**) process 1, (**b**) process 2, and (**c**) process 3. (**d**) Variation in the $ncTiO_2$ crystal size based on XRD data

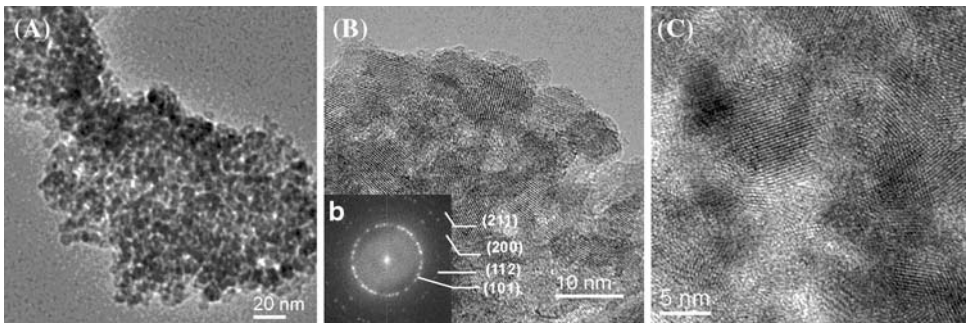

Fig. 2 (**A**, **B**) Typical HRTEM images of TS210 annealed at 773 K, showing well-dispersed $ncTiO_2$ in an SiO_2 matrix. The magnified image in (**B**) shows a well-ordered, long-range nanostructure with a grain size of 7–8 nm. Inset (**b**) is a Fourier-transform image of (**B**) and indicates (101), (122), (200) and (211) anatase reflections, and that most crystal planes are oriented with the (101) plane that most of the crystal planes are oriented with the (101) plane. (**C**) Typical HRTEM image of TS310 annealed at 773 K

$ncTiO_2$ grain size is probably underestimated owing to the fact that the contribution of larger lattice strains to the peak broadening has been neglected.

Typical HRTEM images of TS230 are shown in Fig. 3A–D, with a Fourier-transform image of (B) shown in (b). The images clearly demonstrate that $ncTiO_2$ anatase of grain size approximately 6–10 nm is formed in an amorphous SiO_2 matrix, with poor dispersion of the $ncTiO_2$ as compared to sample TS210 shown in Fig. 2. Furthermore, the lattice defects of the $ncTiO_2$ in the 30 mol% SiO_2 Ti–Si samples are greater than those in the 10 mol% SiO_2 samples. Examples of these are the fringe dislocation in image (B), the crinkle caused by a crystal twin in image (C), and other crystal lattice defects in images (C) and (D), especially in the areas circled. These defects indicate the presence of larger lattice strains in the $ncTiO_2$ for the 30–40% SiO_2 samples. Therefore, it may be inferred that: (1) a further increase in SiO_2 content does not decrease the crystal grain size or promote the dispersion of $ncTiO_2$ in the SiO_2 matrix, but leads to large lattice strains in $ncTiO_2$; and (2) the broad XRD peaks for samples with 30–40 mol% SiO_2 might originate from the larger lattice strains in the $ncTiO_2$. In fact, broadening of XRD peaks caused by crystal lattice defects has attracted the attention of other researchers in the investigation of nanocrystalline (nc) materials [22, 23]. Moreover, these surface defects on $ncTiO_2$ are beneficial for the photocatalytic activity and photoinduced hydrophilicity of TiO_2 [24, 25].

To sum up, the grain growth and dispersion of $ncTiO_2$ anatase in Ti–Si binary oxides may be related to the large lattice strains induced by the introduction of SiO_2 into $ncTiO_2$. This result seems to bear some resemblance to a previous report [26], in which it was postulated that the crystal grain size of CdSe quantum dots was related to the

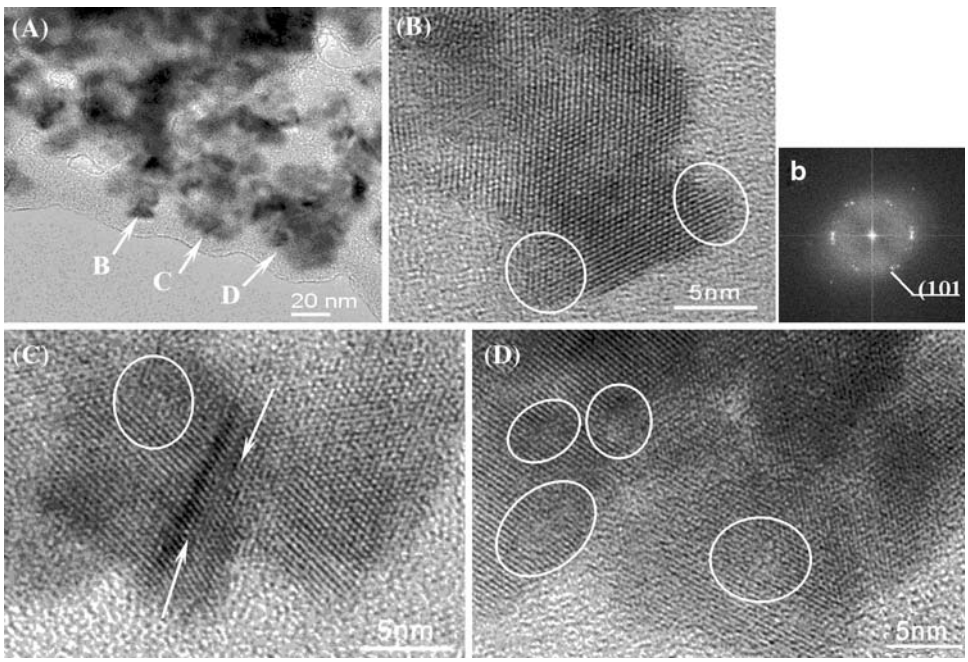

Fig. 3 HRTEM images of TS230 annealed at 773 K showing a grain size of approximately 6–10 nm with various crystal defects. (**A**) Integrated image showing that $ncTiO_2$ is not properly dispersed in the SiO_2 matrix. (**B**–**D**) Magnified local HRTEM images of (**A**): (**B**) fringe dislocation; (**C**) crinkle due to a twin crystal; and (**D**) other crystal defects, especially in the areas circled. (**b**) is a Fourier-transform image of (**B**) indicating the presence of $ncTiO_2$ that is mostly oriented with the anatase (101) plane

lattice strain energy induced by the lattice mismatch between the CdSe and the Au or Pb substrate. To further understand the variation in the lattice strains in $ncTiO_2$, the unit-cell volumes (V) of $ncTiO_2$ anatase produced at different annealing temperatures and with different SiO_2 contents were calculated according to Eq. (2), a formula for the tetragonal system to which anatase belongs. The values obtained are shown in Table 2. For each Ti–Si oxide structure, the trends in the unit-cell volumes with increasing SiO_2 content from 10 to 30 mol% are seen to be somewhat different at the different annealing temperatures. However, most of the unit-cell volumes of $ncTiO_2$ in the three types of Ti–Si binary oxides are distinctly lower than that in pure TiO_2 within the experimental range. The volume shrinkage in $ncTiO_2$ mainly reflects the substitution of Ti^{4+} by Si^{4+} as well as the formation of Ti–O–Si linkages, because the radius of Si^{4+} (0.041 nm) is much smaller than that of Ti^{4+} (0.064 nm), and the Si–O bond (0.159 nm) is much shorter than the Ti–O bond (0.179 nm), while an increase in the unit-cell volume of $ncTiO_2$ might indicate the existence of interstitial Si^{4+}. These findings suggest that in these Ti–Si binary oxides, both substitution of Ti^{4+} by Si^{4+} and interstitial Si^{4+} centers might occur simultaneously in the lattice of $ncTiO_2$ and contribute to the large lattice strains therein, with the former making the dominant contribution. This result is consistent with a previous report that large lattice strains in $ncTiO_2$ could be induced by the substitution of dopant cations having ionic radii greater or smaller than that of Ti^{4+} [27, 28]. In addition, the larger lattice strains in the $ncTiO_2$ samples with 30–40 mol% SiO_2 as compared with that in the 10 mol% SiO_2 samples may be explained in terms of increased substitution of Ti^{4+} by Si^{4+} or an increased amount of interstitial Si^{4+}.

Effect of SiO_2 addition on annealing at 1273 K

X-ray diffraction patterns of Ti–Si binary oxides annealed at 1273 K are shown in Fig. 4a–c. It can be clearly seen that the rutile phase is formed at 1273 K in each of the 10 mol% SiO_2 samples. However, for pure $ncTiO_2$ prepared by the same sol-gel process, the rutile phase only appears at 873 K. This finding indicates that the anatase-rutile transformation (ART) is significantly suppressed by the addition of SiO_2. Furthermore, varying the SiO_2 content allows control of the ART of $ncTiO_2$. To clarify the effect of the three binary oxide structures on the ART of $ncTiO_2$, the rutile contents in the $ncTiO_2$ grains were calculated according to Eq. (3) for the 10 mol% SiO_2 samples. As shown in Fig. 4d, the rutile content in TS210, i.e., intimately mixed silica–titania made by process 2, is much less than that in TS110 or TS 310. This result may indicate that the ART of $ncTiO_2$ is related to the structures of the Ti–Si oxide samples; moreover, using process 2, i.e., to obtain atomically mixed silica–titania, could be the most effective way to suppress the ART of $ncTiO_2$.

The changes in the grain size of $ncTiO_2$ anatase with increasing annealing temperature and SiO_2 content are shown in Table 3. For each of the Ti–Si binary oxides, the $ncTiO_2$ grain size greatly increases with increasing annealing temperature up to 1273 K. However, for Ti–Si oxide samples annealed at 1273 K, the $ncTiO_2$ grain size generally decreases with increasing SiO_2 content from 10 to 30 mol%. The variation in the $ncTiO_2$ grain size among the three Ti–Si oxide structures is greater for the 10 mol% SiO_2 samples than for the 30 mol% SiO_2 samples. Moreover, the smallest grain size is found in TS210, TS220, and TS230, intimately mixed silica–titania samples made by process 2, among the respective 10, 20, and 30 mol% SiO_2 samples annealed at 1273 K. This result suggests that under high-temperature annealing (1273 K): (1) the grain size of $ncTiO_2$ anatase may be controlled by variation of the SiO_2 content; (2) the grain growth of $ncTiO_2$ in Ti–Si oxide samples is related to the composite structure itself, and the use of process 2 could be the best way to limit the grain growth of $ncTiO_2$. Moreover, 30 mol% SiO_2 is optimal for hindering the grain growth of $ncTiO_2$ anatase. In general, it could be deduced that the grain size and ART of $ncTiO_2$ depend not only on the annealing temperature and SiO_2 content, but also on the composite structure.

The exact mechanism that governs the grain growth and ART of $ncTiO_2$ is still not fully understood. However, in many previous reports on doped $ncTiO_2$ [27, 28] and pure $ncTiO_2$ [29, 30], it has been postulated that both the grain growth and ART of $ncTiO_2$ are related to lattice strains therein. In addition, a critical size mechanism for ART in

Table 2 Variation in unit-cell volume (V) for $ncTiO_2$ anatase in the three types of Ti–Si binary oxides

Annealing Temp. (K)	TS110 (nm^3)	TS120 (nm^3)	TS130 (nm^3)	TS210 (nm^3)	TS220 (nm^3)	TS230 (nm^3)	TS310 (nm^3)	TS320 (nm^3)	TS330 (nm^3)	Pure TiO_2 (nm^3)
873	0.1374	0.1369	0.1379	0.1368	0.1359	–	0.1344[a]	0.1361[a]	–	0.1377 (873 K)
1173	*0.1359*	0.1361	0.1361	0.1363	0.1364	0.1354	*0.1360*[b]	0.1354[b]	0.1359[b]	
1273	0.1354	*0.1360*	0.1366	*0.1360*	0.1361	0.1363	0.1364	0.1364	0.1362	

Note: The values marked with a superscript 'a' and 'b' relate to samples annealed at 773 and 1073 K, respectively

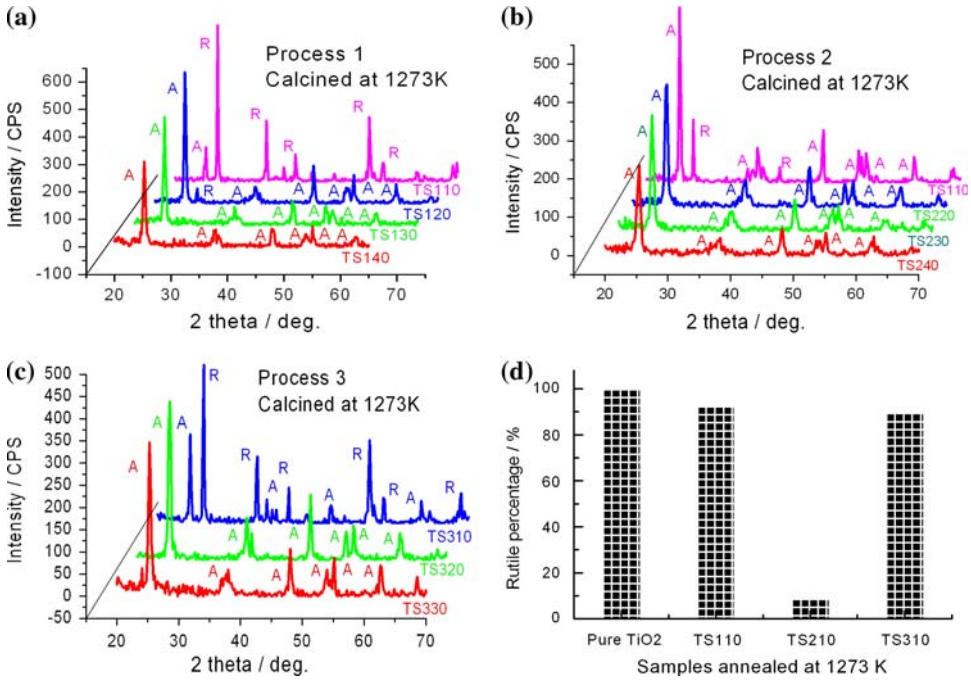

Fig. 4 (**a**, **b**, **c**) XRD patterns of Ti–Si binary oxides annealed at 1273 K: (**a**) process 1; (**b**) process 2; and (**c**) process 3. (**d**) The rutile contents in TS110, TS210, TS310, and pure TiO_2 annealed at 1273 K

Table 3 Variation in grain size of $ncTiO_2$ anatase in the three types of Ti–Si binary oxides.

Annealing Temp. (K)	TS110 (nm)	TS210 (nm)	TS310 (nm)	TS120 (nm)	TS220 (nm)	TS320 (nm)	TS130 (nm)	TS230 (nm)	TS330 (nm)
773	7.90	8.57	7.73	6.90	7.89	7.60	3.47	3.00	3.25
873	8.66	8.75	–	8.26	9.91	–	8.38	7.44	–
1173	21.54	20.60	18.63[a]	15.00	13.31	11.62[a]	10.54	16.07	9.43[a]
1273	59.23	29.50	36.61	25.65	17.67	21.25	19.41	17.07	19.74
ΔV (nm^3)	0.020	*0.008*	0.020	0.009	*0.005*	0.010	0.018	–	–

Note: The values marked with a superscript 'a' relate to samples annealed at 1073 K. ΔV denotes the difference in the $ncTiO_2$ unit-cell volume between the largest and smallest values among the three annealing temperatures of 873, 1173, and 1273 K

TiO_2 and doped TiO_2 has also recently been proposed [31]. To further understand the mechanism that governs the grain growth and ART of $ncTiO_2$ in the three Ti–Si oxide structures, the variation in the lattice strains in the $ncTiO_2$ with increasing annealing temperature has been analyzed on the basis of the variation in the unit-cell volume in the $ncTiO_2$ anatase. It may be noted from Fig. 4 that in four of our Ti–Si samples the rutile phase appeared at an annealing temperature of 1273 K, i.e., TS110, TS120, TS210, and TS310. For TS120 and TS210, the initial formation of rutile nuclei perhaps occurs at an annealing temperature around 1273 K, since their $ncTiO_2$ rutile contents are 5.6 and 8.7 wt%, respectively, at 1273 K, while for TS110 and TS310, the initial formation of rutile nuclei is estimated to occur at about 1173 K, since their rutile contents are 92.5 and 89.6 wt%, respectively, at 1273 K. The variations in the unit-cell volumes in the $ncTiO_2$ anatase in the three Ti–Si oxide structures with increasing annealing temperature are shown in Table 2. It can be seen that the unit-cell volumes of $ncTiO_2$ anatase at the temperature of initial rutile nuclei formation are about 0.1360 nm^3 in each of the four samples. This result might suggest that there is a definite value of the unit-cell volume or lattice strain of $ncTiO_2$ anatase that induces its ART. In addition, this explanation does not contradict the proposed critical size mechanism [31]. As can be seen in Table 3, for TS120 and TS210 at 1273 K the grain sizes of $ncTiO_2$ anatase are 25.65 and 29.50 nm, respectively, while for TS110 and TS 310 at 1173 K they are 21.54 and 18.63 nm, respectively. From this, it can be deduced that the critical grain size of $ncTiO_2$ anatase for the initial ART of $ncTiO_2$ should be less than 25.65 nm and larger than 18.63 nm. This result is in accordance with the above-cited literature report on a critical size mechanism for ART in TiO_2.

For the three Ti–Si oxide structures, the grain growth of $ncTiO_2$ may relate to the thermal behavior of the lattice strain therein, and this behavior may be reflected in the thermal variation of the unit-cell volume of $ncTiO_2$. As

shown in Table 2, on increasing the annealing temperature from 873 to 1273 K, the unit-cell volume of $ncTiO_2$ anatase generally decreases for silica-supported titania, varies slightly for intimately mixed silica–titania, and increases for silica-coated titania, with the exception of TS230. For the first two Ti–Si oxide structures, the trends in the unit-cell volumes are not consistent with that of pure $ncTiO_2$ [32], in which the unit-cell volume of $ncTiO_2$ anatase increases with increasing annealing temperature due to thermal expansion. These variations indicate that the thermal behavior of the lattice strains in $ncTiO_2$ is related to the structures of the Ti–Si oxides. In addition, to further understand the relationship between the thermal variation of the unit-cell volume and the grain growth of $ncTiO_2$ anatase, the differences in the unit-cell volumes (ΔV) between the largest and smallest values for the three annealing temperatures of 873, 1173, and 1273 K were calculated from the data in Table 2. For the sake of comparison, these differences (ΔV) are shown in Table 3. It can be noted that the differences (ΔV) for TS210 and TS220, intimately mixed silica–titania made by process 2, are the smallest for the 10 and 20 mol% SiO_2 samples, respectively. The small variations in the unit-cell volume of $ncTiO_2$ anatase for TS210 and TS220 may indicate that the thermal variation of lattice strain in $ncTiO_2$ anatase is small for intimately mixed silica–titania. Therefore, the best inhibition of $ncTiO_2$ grain growth seen for intimately mixed silica–titania may relate to the small thermal variation of the lattice strains therein.

Information about the microstructure and dispersion of $ncTiO_2$ anatase in a SiO_2 matrix at a high annealing temperature can be gleaned from Fig. 5, which shows typical HRTEM images of TS230 annealed at 1173 K. It can be clearly seen that the Ti–Si composite particles have been sintered together in the process of calcination. However, the corn-like $ncTiO_2$ anatase grains of approximate size 20 nm are well dispersed in the amorphous SiO_2 matrix, and few defects are observed in these crystallites possibly due to relaxation of the structure. The grain size of this $ncTiO_2$ is slightly larger than 16.07 nm, the grain size calculated from XRD data for the same sample. This result indicates that the nanosized crystallites of TiO_2 anatase were well dispersed in the SiO_2 amorphous matrix at a high annealing temperature of 1173 K.

Conclusion

For each of the Ti–Si binary oxides annealed at 773 K, addition of 10 mol% SiO_2 sharply decreases the grain size of $ncTiO_2$ anatase to 7–8 nm and leads to well-dispersed $ncTiO_2$ in the amorphous SiO_2 matrix as compared with pure $ncTiO_2$. A further increase in the SiO_2 content to 30 mol% does not decrease the crystal grain size or promote the dispersion, but leads to more crystal defects in the $ncTiO_2$ anatase. Furthermore, there are no significant differences in the initial grain growth of $ncTiO_2$ anatase among the three types of Ti–Si binary oxides. However, with increasing annealing temperature up to 1273 K, the grain growth and ART of $ncTiO_2$ depend not only on the annealing temperature and SiO_2 content, but also on the composite structure. Both the grain growth and ART of $ncTiO_2$ are greatly suppressed by increasing SiO_2 content for all of the Ti–Si binary oxides, and intimately mixed silica–titania shows the best inhibitory effect in these two respects among the three Ti–Si structures. The differences between the three Ti–Si oxide structures might be attributed to variation in the large lattice strains in the $ncTiO_2$. The large lattice strains in $ncTiO_2$ could result from both the substitution of Ti^{4+} by Si^{4+} and the presence of interstitial Si^{4+}, but the former plays a dominant role since all unit-cell volumes of $ncTiO_2$ anatase for Ti–Si binary oxides are smaller than that for pure TiO_2. For the three types of Ti–Si binary oxides, there may be a definite value for the unit-cell volume of $ncTiO_2$ anatase that induces its ART. The best inhibitory effect on the grain growth of $ncTiO_2$ anatase seen for intimately mixed silica–titania might result from the small thermal variation in the $ncTiO_2$ unit-cell volume. For

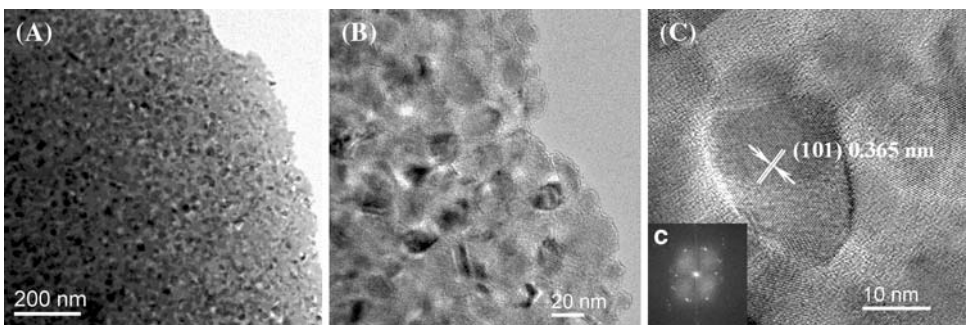

Fig. 5 HRTEM images of TS230 annealed at 1173 K. (**A**) TiO_2 crystallites homogeneously dispersed in an amorphous SiO_2 matrix. (**B**) Magnified image showing that the average grain size of TiO_2 is approximately 20 nm. (**C**) Magnified image showing corn-like $ncTiO_2$ with inset (**c**) Fourier-transform image of (**C**), which indicates the $ncTiO_2$ is anatase

all Ti–Si binary oxides annealed at 1273 K, variation of the SiO_2 content allows control over the grain growth and ART of $ncTiO_2$, and 30 mol% SiO_2 proved to be optimal for hindering the grain growth of $ncTiO_2$ anatase.

Acknowledgements Financial support from the Natural Science Foundation of China (grant numbers 20476067 and 90306014) is gratefully acknowledged. The authors would like to thank the staff of the Key Laboratory of Interfaces and Engineering in Advanced Materials and the Key Laboratory of Coal Science and Technology, for their help in performing the HRTEM and XRD measurements.

References

1. Hu C, Tang YC, Yu JC, Wong PK (2003) Appl Catal B 40:131
2. Muhammad SV, Keiichi T (2003) Water Res 37:3992
3. Ismail AA, Ibrahim IA, Ahmed MS, Mohamed RM, Eishall HJ (2004) Photochem Photobiol A 163:445
4. Uchiyama H, Suzuki K, Oaki Y, Imai H (2005) Mater Sci Eng B 123:248
5. Xu YM, Zheng W, Liu WP (1999) J Photochem Photobiol A 122:57
6. Cheng SF, Tsai SJ, Lee YF (1995) Catal Today 26:87
7. Chen YX, Wang K, Lou LP (2004) J Photochem Photobiol A 163:281
8. Kobayashi M, Kuma R, Masaki S, Sugishima N (2005) Appl Catal B 60:173
9. Anpo M, Takeuchi M (2003) J Catal 216:505
10. Tanaka T, Teramura K, Yamamoto T, Takenaka S, Yoshida S, Funabiki T (2002) Photochem Photobiol A 148:277
11. Liu ZY, Quan X, Fu HB, Li XY, Yang K (2004) Appl Catal B 52:33
12. Li ZJ, Hou B, Xu Y, Wu D, Sun YH (2005) J Colloid Interface Sci 288:149
13. Miyashita K, Kuroda S, Ubukata T, Ozawa T, Kubota H (2001) J Mater Sci 36:3877. doi:10.1023/A:1017901717571
14. Arai Y, Tanaka K, Khlaifat AL (2006) J Mol Catal A 243:85
15. Wilhelm P, Stephan D (2007) J Photochem Photobiol A 185:19
16. Mei F, Liu C, Zhang L, Ren F, Zhou L, Zhao WK, Fang YL (2006) J Cryst Growth 292:87
17. Dutoit DCM, Schneider M, Baiker A (1995) J Catal 153:165
18. Liu AH, Liu PG (2003) Principle and application of x-ray diffraction. Chemical Industry Press House, Beijing, pp 31, 211
19. Spurr RA, Myers H (1957) Anal Chem 29:760
20. Gunji T, Kasahara T, Abe Y (1998) J Sol-Gel Sci Technol 13:975
21. Suryanarayana C (2001) Prog Mater Sci 46:1
22. Eastman JA, Beno MA, Knapp OS, Thompson LJ (1995) Nanostruct Mater 6:543
23. Fitzsimmons MA, Eastman JA, Robinson RA, Lawson AC, Thompson JD, Movshovich R, Satti J (1993) Phys Rev B 48:8245
24. Takeuchi M, Onozaki Y, Matsumura Y, Uchida H, Kuji T (2003) Nucl Instrum Meth B 206:259
25. Liu H, Ma HT, Li XZ, Li WZ, Wu M, Bao XH (2003) Chemosphere 50:39
26. Golan Y, Hodes G, Rubinstein I (1996) J Phys Chem 100:2220
27. Kim J, Song KC, Foncillas S, Pratsinis SE (2001) J Eur Ceram Soc 21:2863
28. Rodríguez-Talavera R, Vargas S, Arroyo-Murillo R, Montiel-Campos R, Haro-Poniatowski E (1997) J Mater Res 12:439
29. Apatiga LM, Rivera E, Castano VM (2007) J Am Ceram Soc 90:932
30. Sun YJ, Egawa T, Zhang LG, Yao X (2002) Jpn J Appl Phys 41:L945
31. Reidy DJ, Holmes JD, Morris MA (2006) J Eur Ceram Soc 26:1527
32. Neelam J, Mahesh B, Preeti A, Veda R (2005) Thermochim Acta 427:37